nature physics

Article

https://doi.org/10.1038/s41567-023-02053-z

Flat band separation and robust spin Berry curvature in bilayer kagome metals

In the format provided by the authors and unedited

nature physics

Article

https://doi.org/10.1038/s41567-023-02053-z

Flat band separation and robust spin Berry curvature in bilayer kagome metals

In the format provided by the authors and unedited

CONTENTS

SAMPLE PREPARATION FOR ARPES MEASUREMENTS

The samples were glued onto a copper sample holder by using silver epoxy and they were top-posted with a ceramic post. Then, they were cleave in ultrahigh vacuum (UHV) at the base pressure 1×10^{-10} mbar. This ensures the presence of a fresh surface, that allows for the surface states to be detected. The measurements were performed at 16 K and at 77 K, in both cases for all of the samples shown in the main text, a non-magnetic phase was measured.

For all samples, we performed ARPES by using linearly polarized light, both horizontal and vertical. The former, with respect to the sample mirror plane, couples to both odd and even components of the orbitals (with equal contribution), while the latter only to the even components. The use of various polarization, as we also show in the main text, enables different bands to be seen: features such as the quadratic minimum (QM) of the itinerant bands or the flat bands are highlighted selectively by changing the light polarization. Also when one uses circularly polarized light, this argument holds and the identification of the topological features in the spectra could be more challenging. In order to be sure of our results and the attribution of topological character to QM, we additionally made a comparison between both linear polarizations and circular polarization which reveals that linear horizontal light has common features with circular polarization, thus the flat band shows up only in the spectra collected with linear vertically polarized light. This allows us to attribute the finite spin-Berry curvature signal to the QM (See Fig.1).

SURFACE TERMINATIONS

The XV_6Sn_6 kagome metals have already shown the presence of two possible cleavage planes, i.e. one with Sn and one with V termination (which features a kagome atomic arrangement). We found these terminations to be very large and comparable at least to the beam spot size of the laboratory NFFA APE-LE (150×50 μm^2), and clearly identified by the Sn core levels, as we showed in Fig.1 of the main text.

From the core levels, it is straightforward to identify the type of termination. Furthermore, the spectral features obtained for such terminations are rather different, both in terms of Fermi surface maps (Fig. 2) and of energy-vs-momentum dispersions (Fig. 3). In addition to the results given in Fig.1 of the main text, we here show the Fermi surfaces obtained by density-functional theory (DFT) calculations, which provide a satisfactory agreement with the experiment (Fig. 2).

As we discussed in the main text, we stress that the topological surface states in the XV_6Sn_6 kagome metals belong to the Sn termination. However, the measurements of the spin-Berry curvature is termination independent, because the topological gap opens between the bulk flat and itinerant states upon the action of spin-orbit coupling (SOC).

f-LEVELS OF TERBIUM IN TbV_6Sn_6 AND THE TIME-REVERSAL SYMMETRY

TbV_6Sn_6 undergoes a magnetic transition at low temperature ($<$5K). Therefore, in order to perform the spin-Berry curvature measurements on this system preserving time-reversal symmetry, we performed all our measurements above the critical temperature, *i.e.* at 16 K and at 77 K, without finding any difference between the two cases. In addition to this, we also used ARPES to identify the binding energy of the f-levels of Tb, which enable the sample to have a magnetic transition. We found that these are located well below the Fermi energy (E-E_F=[-10,-7] eV), thus, in any case, showing a negligible hybridization with the near-Fermi electronic structure of this compound (see Fig. 4).

The presence of time-reversal symmetry is also reflected by the spin-reversal observed in the surface states of the Sn-terminated surface of TbV_6Sn_6. As shown in Fig. 4 of the main text, the time-reversal symmetry constraint is preserved and visible with the spin-polarization reversal from $+k$ to $-k$. For visualization purposes and sake of completeness, we also show here the same result in the form of spin up/down difference-maps in Fig. 5 for the S_y component of the spin.

THE CHARGE DENSITY WAVE IN ScV_6Sn_6

ScV_6Sn_6 is the only member of the 166-family kagome metal which exhibits a charge density wave (CDW) transition. Such a CDW is different from the one reported for the 135 sister compounds and allows us to study the robustness of the topological properties after the charge order has occurred. As we showed in the main text, the topology remains robust and unaffected by the CDW, potentially allowing the many-body ground state and the topological character of ScV_6Sn_6 to be engineered separately. For completeness to the data on the spin-Berry curvature reported in the main text, here we show the ARPES measurements collected with both light polarizations. In particular, Fig. 6 presents the Fermi surface maps and the energy-momentum dispersions. In addition, in Fig. 7, we report susceptibility measurements on ScV_6Sn_6 demonstrating a clear phase

transition (onset of CDW) at 98 K.

ROBUST SPIN-BERRY CURVATURE ACROSS THE TRANSITION OF ScV_6Sn_6

In order to investigate the robustness of the topological properties of ScV_6Sn_6 against perturbations, we exploited the intrinsic CDW transition hosted by this material. Thus, we collected spin-Berry curvature data above and below the transition temperature ($\sim$92 K). The data, shown in supplementary figure 10, show the measurements of the topological gap in ScV_6Sn_6 upon setting of the CDW. Below the temperature (at 16 K - Fig. 10**a**-**b**) the spin-resolved circular dichroism reveals a finite contribution which reverses sign with the sign of the spin species, confirming also the maintenance of the time-reversal symmetry. The same behaviour is observed above the transition (130 K – Fig. 10**c**-**d**), and this reflects the robust character of the topology of the flat band and quadratic minimum. The data have been collected under the same experimental conditions, at 78 eV photon energy and with both components of the out-of-plane spins. Apart from a general increase in the noise due to the increased thermal broadening of the data above the transition temperature, the trend is the same and the spin-Berry curvature is robust against the CDW symmetry breaking.

DETAILS ON THE SPIN-ARPES ANALYSIS

The spin-data presented in the main text have undergone the following procedure in order to extract what in the spin-ARPES community is known as 'true spin-polarization' – Note that the exact same conclusion and behaviour is visible in the raw data without any processing at all, so our procedure does not compromise at all the validity of the experimental results and it is limited only to a standard and well-accepted methodology [See also Riley et al., Nat. Phys. **10**, 835, (2014) and Bawden et al., Nat. Communs. **7**, 11711, (2016)].

First of all, the raw data for spin-up and spin-down channels have been normalised to their background (unpolarised component), such that the background matched in both cases. In the present study, the background normalisation was easy because its signal of the two-spin species was lining up already very well and the normalisation consisted only of a multiplication as high as 1.01 for one spin EDC to be perfectly matched to that one of the opposite spin channel. After

normalisation, in order to extract what is known as "true spin polarisation", we used the following relationships:

$$I^{TRUE}(k,\uparrow) = \frac{I^{TOT}(k)}{2} * (1+P)$$

$$I^{TRUE}(k,\downarrow) = \frac{I^{TOT}(k)}{2} * (1-P)$$

where P is the polarization of the system and $I^{TOT} = I^{bg.norm}(k,\uparrow) + I^{bg.norm}(k,\downarrow)$ is simply the sum of the intensity for EDCs with spin up and spin down after normalisation to the background. The Polarisation P includes, as it should the Sherman function from the instrument (i.e. η=0.3) and is described by:

$$P(k) = \frac{1}{\eta} * \frac{I^{bg.norm}(k,\uparrow) - I^{bg.norm}(k,\downarrow)}{I^{bg.norm}(k,\uparrow) + I^{bg.norm}(k,\downarrow)}$$

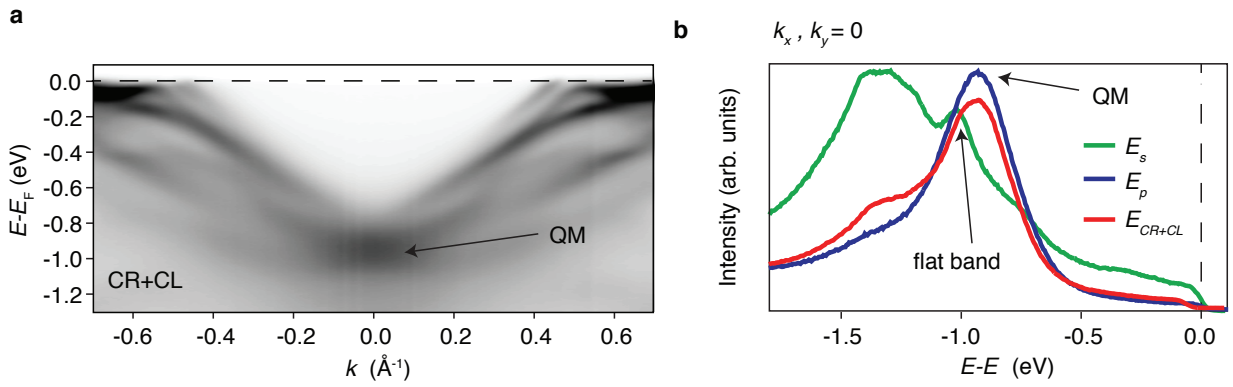

FIG. 1. **Matrix elements, flat and itinerant bands.** **a** ARPES energy-momentum dispersion collected by using circularly polarized light and summed up for right and left handed polarizations. The quadratic minimum (QM) is clearly identified in the spectra. **b** Energy distribution curves at the zone centre are compared for all light polarization vectors. The signal for circularly polarized light is similar to that from linear horizontal light polarization, thus allowing us to visualize the quadratic minimum. On the contrary, the linear vertical polarization, as also shown in the main text, is only sensitive to the flat band intensity.

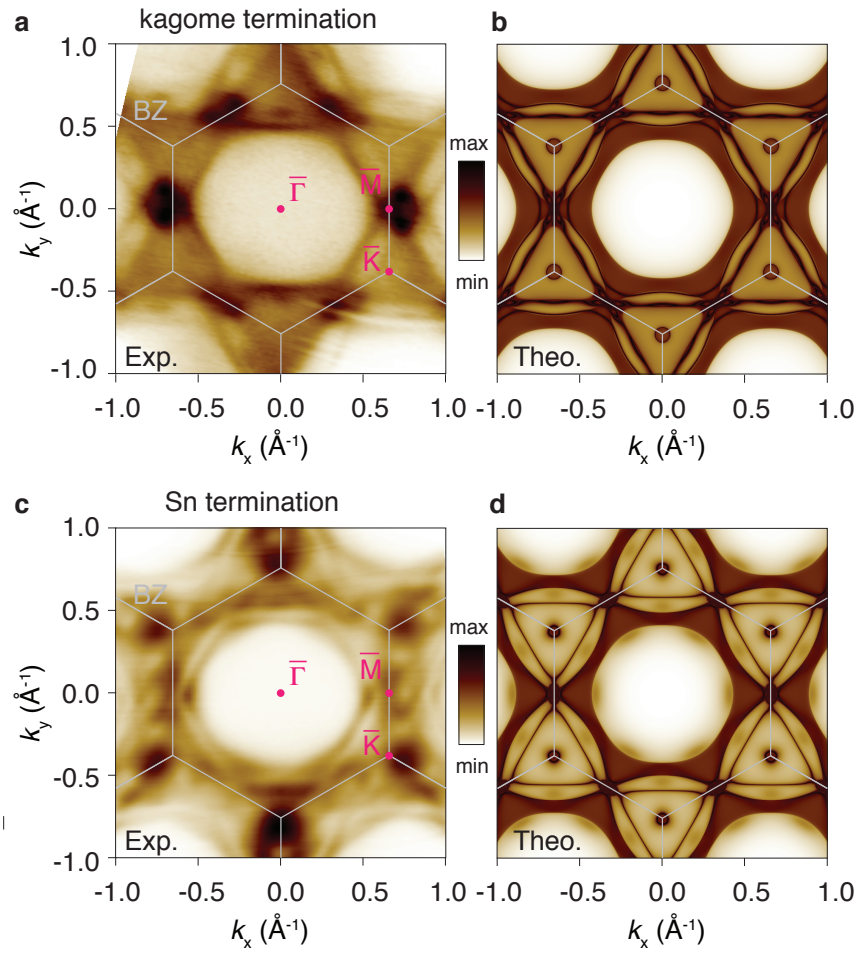

FIG. 2. **Fermi surfaces of TbV_6Sn_6 kagome metal.** **a** Experimental and **b** theoretical Fermi surface of TbV_6Sn_6 expected for the kagome termination. **c** Experimental and **d** theoretical Fermi surface of TbV_6Sn_6 expected for the Sn termination. In both cases, the kagome motif, which is a prerogative of the bulk electronic structure is visible. The experimental spectra have been plotted to account for the correct contribution of both light polarizations.

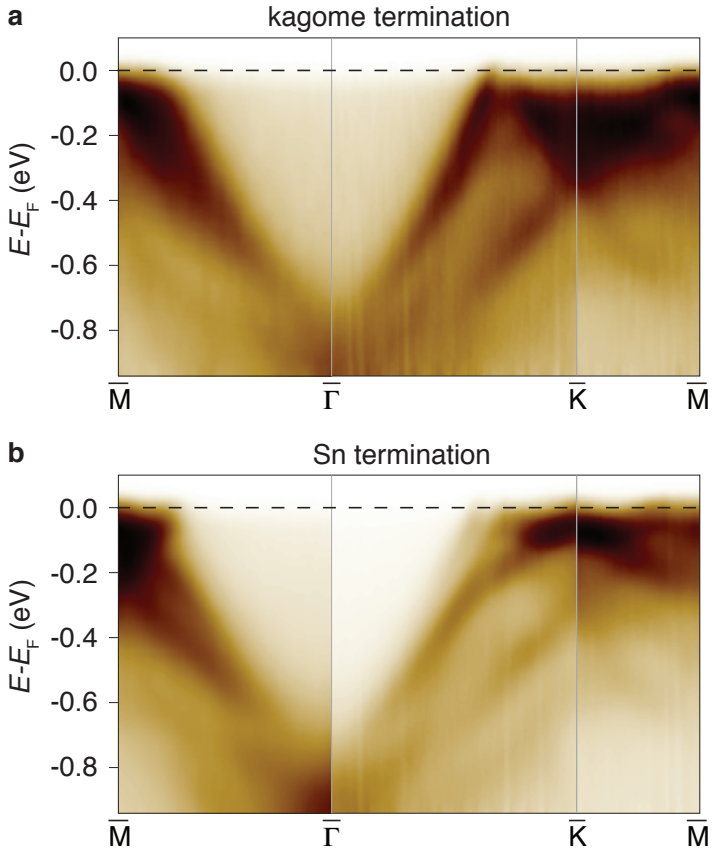

FIG. 3. **Terminations of TbV_6Sn_6 and electronic structure.** Energy-momentum dispersions obtained by ARPES for **a** kagome and **b** Sn terminations. The experimental spectra have been plotted to account for the correct contribution of both light polarizations.

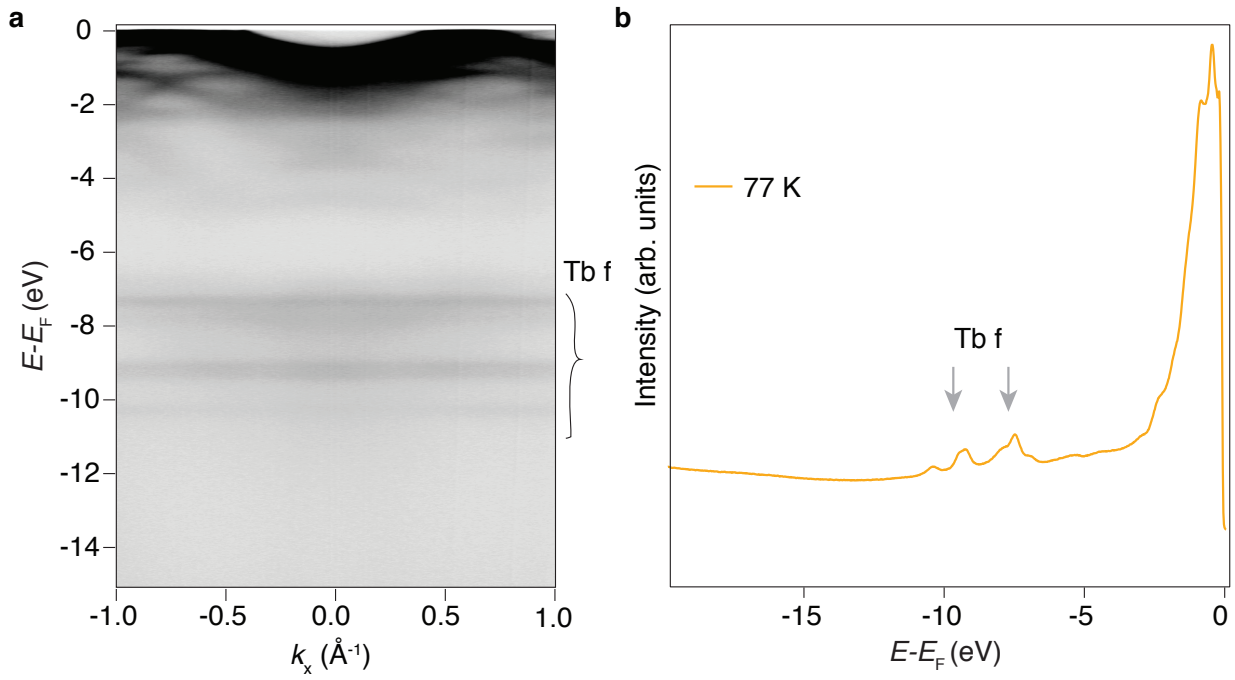

FIG. 4. **TbV_6Sn_6 wide energy range.** **a** Electronic structure spectrum showing also the $4f$ core levels of Tb below 7 eV of binding energy. **b** Integrated intensity obtained from **a**, which gives a complementary view on the high energy range of the $4f$ Tb core levels.

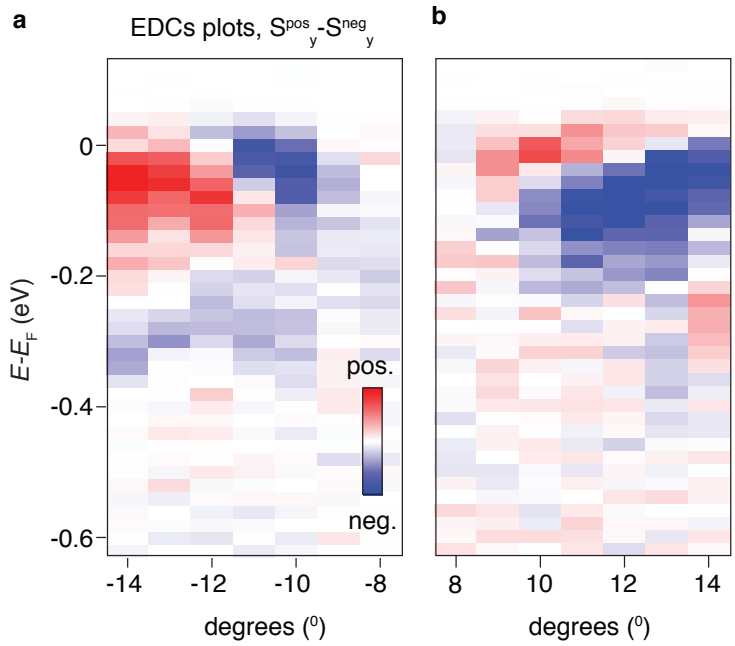

FIG. 5. **TbV_6Sn_6 EDCs resolved in spin**. **a** EDCs resolved in spins for negative values of photoemission angles and for **b** positive values of the angles. The used photon energy0 was 75 eV.

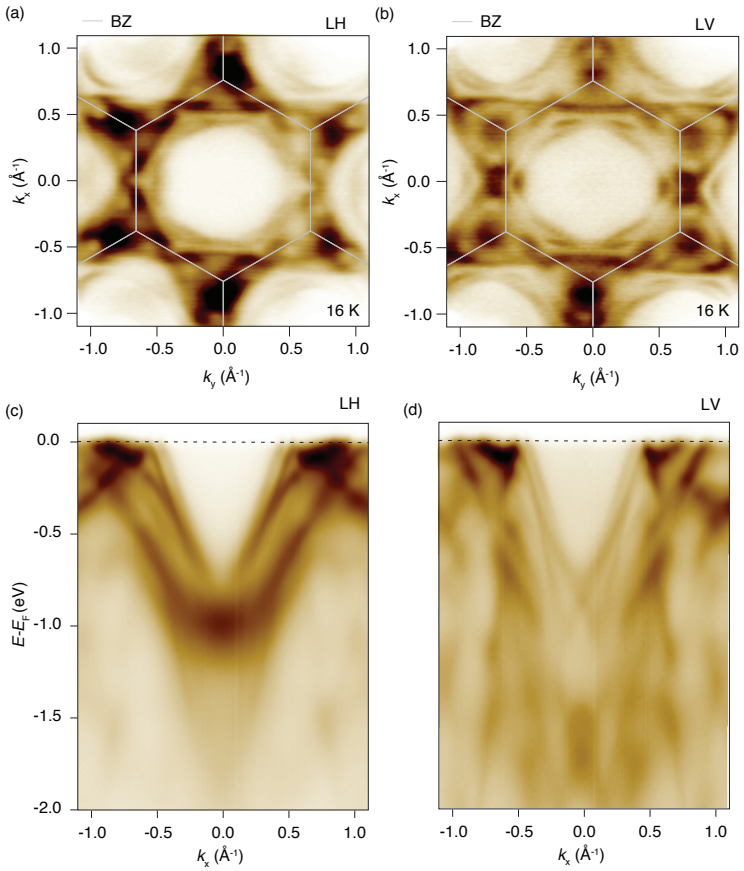

FIG. 6. **ARPES on ScV_6Sn_6.** Fermi surface of ScV_6Sn_6 collected with 75 eV and with **a** linear horizontal and **b** linear vertical polarization. The hexagonal Brillouin zone is indicated by the grey lines. **c** Linear horizontal and **d** linear vertical polarization spectra showing the energy-vs-momentum dispersion along the Γ-K (k_x) direction.

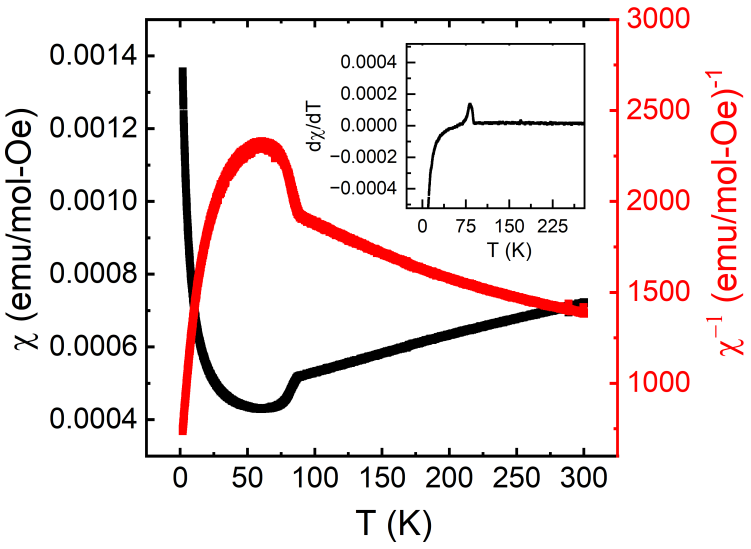

FIG. 7. **CDW in ScV_6Sn_6.** Temperature-dependent magnetization data for ScV_6Sn_6 plotted as magnetic susceptibility, $\chi = M/H$, and inverse magnetic susceptibility, χ^{-1}, collected under a 1 Tesla applied magnetic field parallel to the crystal surface. The inset shows the $d\chi/dT$ as a function of temperature around the CDW transition.

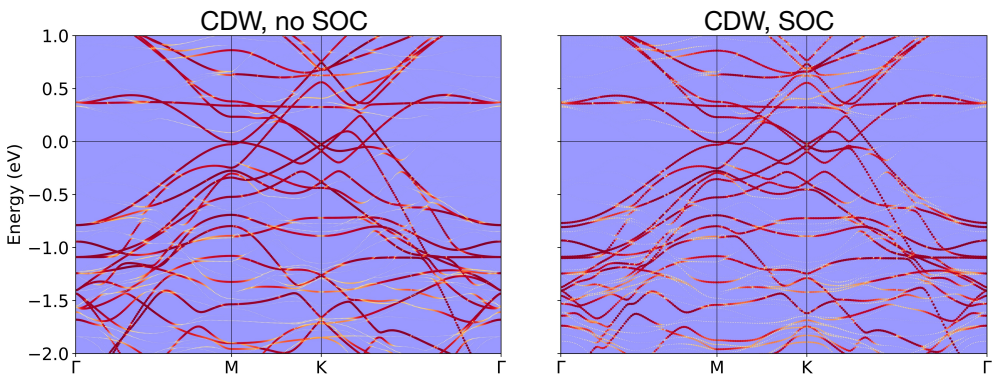

FIG. 8. **CDW in ScV_6Sn_6.** DFT bandstructure of distorted ScV_6Sn_6, with and without SOC, upon unfolding into the primitive Brillouin zone. The two plots clearly demonstrate that the CDW does not sensibly affect the electronic properties of ScV_6Sn_6.

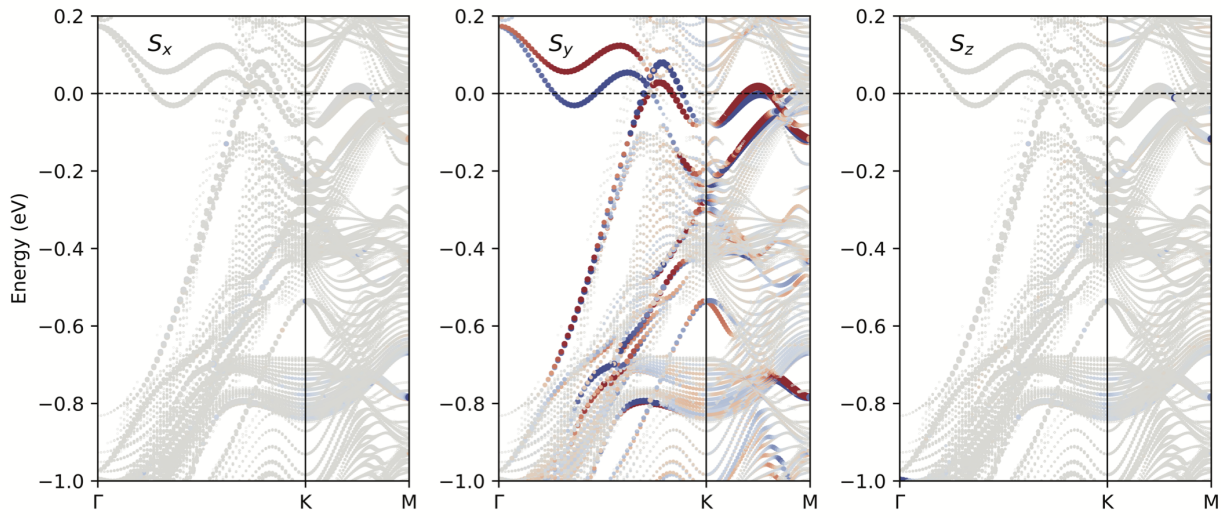

FIG. 9. **Spin texture of topological surface states along all directions.** DFT electronic structure of the Sn surface termination of a finite TbV_6Sn_6 slab along the k_x direction, where the electronic states are colored by their S_x, S_y, and S_z character. The spin-momentum locking is demonstrated by S_y being the only non vanishing component of the spin vector.

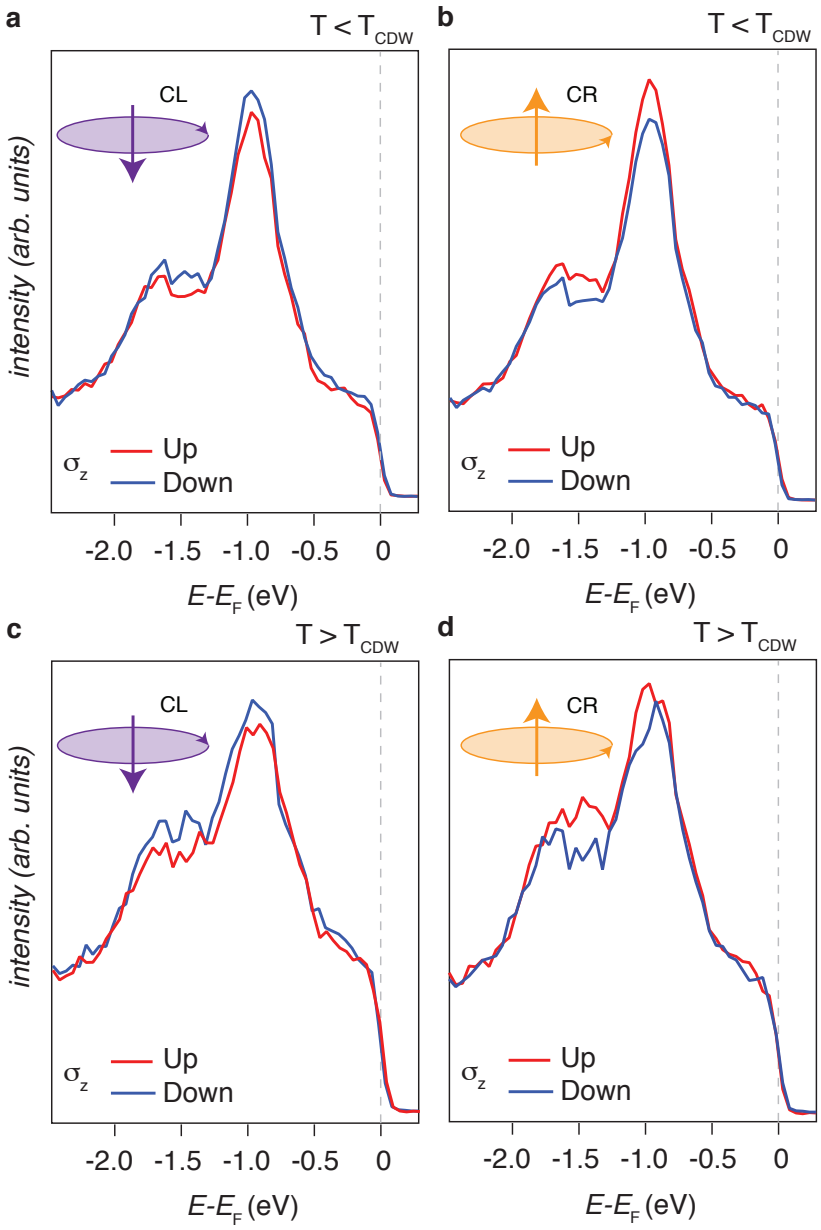

FIG. 10. **Spin-Berry curvature of ScV_6Sn_6 across T_{CDW}.** Spin-resolved EDC (up spins red, down spins blue) collected by using **a** left- and **b** right-circularly polarized light below the transition temperature of the CDW of ScV_6Sn_6 (T=16 K). Spin-resolved EDC (up spins red, down spins blue) collected by using **c** left- and **d** right-circularly polarized light above the transition temperature of the CDW of ScV_6Sn_6 (T=130 K). Apart from the increase in the noise level due to thermal broadening, the spectra remain the same. This corroborates the robustness of the spin-Berry curvature of this compound.